

See discussions, stats, and author profiles for this publication at: <https://www.researchgate.net/publication/278788438>

Polarized Water Wires under Confinement in Chiral Channels

ARTICLE *in* THE JOURNAL OF PHYSICAL CHEMISTRY B · JUNE 2015

Impact Factor: 3.3 · DOI: 10.1021/acs.jpcb.5b03322 · Source: PubMed

READS

21

6 AUTHORS, INCLUDING:



[Yann Le Duc](#)

University of Angers

11 PUBLICATIONS 80 CITATIONS

[SEE PROFILE](#)



[Yves-Marie Legrand](#)

Université de Montpellier

61 PUBLICATIONS 500 CITATIONS

[SEE PROFILE](#)

Polarized Water Wires under Confinement in Chiral Channels

Mihail Barboiu,^{*,†} Pierre-André Cazade,[§] Yann Le Duc,[†] Yves-Marie Legrand,[†] Arie van der Lee,[†] and Benoit Coasne^{*,‡,§}

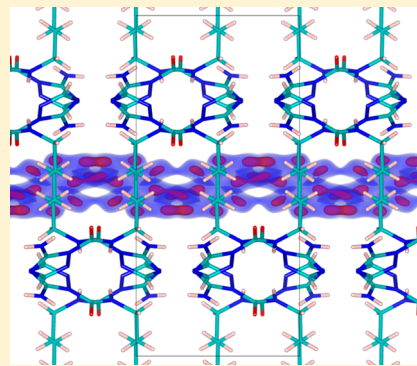
[†]Adaptive Supramolecular Nanosystems Group, Institut Européen des Membranes, ENSCM-UM-UMR-CNRS5635, Place Eugène Bataillon CC047, 34095 Montpellier Cedex 5, France

[‡]Institut Charles Gerhardt Montpellier (ICGM), UMR 5253 CNRS/ENSCM/Université Montpellier 2, 8 rue de l'Ecole Normale, F-34296 Montpellier, France

[§]MultiScale Materials Science for Energy and Environment, UMI 3466 CNRS-MIT and Department of Civil and Environmental Engineering, Massachusetts Institute of Technology, Cambridge, Massachusetts 02139, United States

S Supporting Information

ABSTRACT: The alignment of water molecules along chiral pores may activate proton/ion conduction along dipolar hydrophilic pathways. Here we show that a simple synthetic “T-channel” forms a directional pore with its carbonyl moieties solvated by chiral helical water wires. Atom-scale simulations and experimental crystallographic assays reveal a dynamical structure of water and electrolyte solutions (alkali metal chlorides) confined in these organic T-channels. Oscillations in the dipole orientation, which correspond to alternative ordering (dipole up–dipole down) of the water molecules with a period of about 4.2 Å (imposed by the distance between two successive carbonyl groups) are observed. When ions are added to the system, despite the strong Coulombic water/ion interaction, confined water remains significantly ordered in the T-channel and still exhibits surface-induced polarization. Cation permeation can be achieved through alternated hydration–dehydration occurring along strongly oriented water wires. The T-channel, which exhibits chirality with strong water orientation, provides an opportunity to unravel novel water-channel systems that share many interesting properties of biomolecular systems.



1. INTRODUCTION

Selective exchange of water, ions, and molecules between cells and their surrounding environment is at the heart of many biological processes. As far as transport along biological channels is concerned, the protein structure helps overcome the high energy barrier of translocation of metabolites that may be synergistically transported across the bilayer membrane.¹ In such complex transport problems, electrostatic interactions are known to play a key role in the functional properties of Gramicidin A,^{2,3} Aquaporin,^{4,5} KCsAK⁺,⁶ and M2-Influenza A^{7–9} protein channels. Water is also known to play a crucial role, owing to its complex behavior at the molecular level.^{10–12} Of particular interest, the orientational and positional ordering of water molecules induced by the atomic pore structure and water–water interactions can control ionic conduction as well as ion-valence selectivity and may also prevail in the selective translocation of protons/ions through protein channels.^{2,4,6,7}

Molecular encapsulation of water in man-made materials allows exploring the behavior of water in conditions relevant to confined biological water as well as that of water with reduced dynamics in between those for liquid water and ice.^{13–18} Nevertheless, only a few biomimetic membranes have been considered to selectively and efficiently conduct water.^{19–22} Within this context, unraveling the molecular dynamics of water trapped in artificial host channels is crucial for many scenarios

relevant to biology, physics, chemistry, etc. Specific interaction of water wires with chiral synthetic pores may align the water molecules along their inner chiral surfaces, therefore presenting unique dipolar orientations.^{19–21} The chiro-induced dipolar moment of water wires is of great interest for electrostatic pumping within channels. It may also help design novel devices to mimic protein channels and describe new scenarios of the polarization of chiral biological surfaces biolubricated with electrostatically active dipolar water aggregates.

We recently discovered that a bola-amphiphile bis-triazole compound (TCT) forms self-assembly structures that consist of stable helical pores.²² The TCT forms stable T-channels in lipid bilayers with the hydrated carbonyl and amine moieties pointing toward the interior of the T-channel. Such pores possess diastereoisomeric chiral inner hypersurfaces with atomic details inducing strong orientational ordering of confined water (Figure 1). Experiments have shown that such a T-channel leads to high water flux, high cation/anion selectivity, and large open channel-conductance states when used as bilayer membranes.²² These observations have raised the following issues: (a) the role of such oriented water,

Received: April 6, 2015

Revised: June 9, 2015

Published: June 19, 2015



especially its contribution to ion encapsulation and translocation through the T-channels, and (b) the stability of such confined water, especially under competitive cation–water transport. Here we build on our previous work with an advanced structural and theoretical analysis of water and ion dynamics within the T-channels. We observe that the T-channels associate supramolecular chirality with water alignment along the channels. As in the case of Gramicidin A, our results suggest that ion transport within the T-channels is governed by the subtle balance between hydration and complexation energies of the confined cations. Nevertheless, the large transport activities for the T-channel with respect to Gramicidin A suggests that the dipolar orientation of confined water acts as a lubricant for ion conduction.

2. METHODS

2.1. X-ray Crystal Data. X-ray data were collected on an Agilent Technologies Gemini-S diffractometer using graphite monochromated Mo radiation at 173 K. The structure was easily solved by the *ab initio* charge flipping method using locally normalized structure factors as implemented in the program *Superflip*.²³ The structure could be refined down to $R_1(I > 2\sigma(I)) = 0.0815$ and $wR_2(I > 2\sigma(I)) = 0.0812$. Refinements were carried out using nonlinear least-squares methods within CRYSTALS.²⁴ Because the analysis of the structure showed empty T-channels with a total solvent accessible volume of 478 Å³, representing 23% of the total unit cell volume it was decided to inspect closely the inner contents of the T-channels. By assigning the major peaks in the difference Fourier maps to oxygen atoms and letting the occupancy of these atoms freely refine while keeping constrained to each other the isotropic displacement parameter, the model could be further refined with soft shift limiting restraints to $I > 2\sigma(I) = 0.0485$ and $I > 2\sigma(I) = 0.0330$. The total occupancy of the 8 oxygen positions was 0.7528 corresponding to 6.0 water molecules in the unit cell with an overall isotropic displacement factor somewhat (0.066 Å²) higher than the average isotropic displacement parameter of the TCT molecule itself (0.035 Å²). The total electron count of the unit cell water molecules amounts thus to 60 electrons. Alternatively, the electron density in the unit cell was modeled using the squeeze procedure²⁵ in the program PLATON.²⁶ This yielded 44 electrons in the unit cell, lower than the electron count resulting from the *ad-hoc* refinement of the peaks in the electron density map. The electron count resulting from the refinement of the site occupancy factors may, however, be slightly overestimated because of the high average atomic displacement parameter. The final agreement factors of the refinement using the squeeze-modified structure factors were $I > 2\sigma(I) = 0.0402$ and $I > 2\sigma(I) = 0.0431$.

2.2. Cation Transport Experiments. A volume of 100 μL of vesicles filled with pyranine (8-hydroxypyrene-1,3,6-trisulfonic acid trisodium salt or HPTS) was suspended in 1.9 mL of a phosphate/sulfate buffer. HPTS emission at the wavelength $\lambda = 510$ nm was probed using simultaneous excitation wavelengths equal to 403 and 460 nm. In the course of these experiments, a stock solution containing the compound TCT in 20 μL of DMSO (final solution with concentrations equal to 0.10, 0.20, and 0.40 mM, Table S1, Supporting Information) was added at a time $t = 0$ s. Such additions were followed by the addition of 21 μL of aqueous NaOH (concentration 0.5 M) at a time $t = 60$ s. NaOH increases the pH by about 1 pH unit in the buffer. Important

dye emission modifications were observed at a time $t = 500$ s by lysis of the liposomes with a detergent consisting of 40 μL of aqueous (5%) Triton X100. Transport trace was estimated as the ratio of the intensities emitted at 460 and 403 nm. Rate constants were estimated using the slopes of $\ln([H^+_{in}] - [H^+_{out}])$ as a function of time, where $[H^+_{in}]$ and $[H^+_{out}]$ are respectively the intravesicular/extravesicular proton concentrations. $[H^+_{out}]$ was supposed to be constant over the duration of the experiment, whereas $[H^+_{in}]$ was estimated at each time from the HPTS emission intensities using the calibration relationship, $pH = 1.1684 \cdot \log(I_0/I_1) + 6.9807$. In this equation, I_0 and I_1 are the intensities emitted with the excitation wavelengths 460 and 403 nm, respectively.²⁷

2.3. Molecular Simulation. The material is a monoclinic crystal whose space group is $I12/a1$. The cell parameters are $a = 8.47$ Å, $b = 17.55$ Å, $c = 13.55$ Å with $\beta = 95.85^\circ$. We considered a simulation box of $3 \times 2 \times 2$ replicas along the cell axes (Figure S1a, Supporting Information). The atomic partial charges of the material were estimated in the frame of the Mulliken approach from DFT calculations (B3LYP/6-21G) performed with the software CRYSTAL 06.²⁸ This software, which considers periodic systems, is well adapted for crystalline structures. Thanks to symmetry operations, only 22 out of the 176 atoms in the unit cell are needed to perform the calculations (Figure S1b, Supporting Information).

The experimental structure was kept frozen while performing the quantum chemistry calculations of the electronic energy (i.e., the cell parameters and atomic positions were not optimized). The charges obtained in the present work are in good agreement with those used in the AMBER force field (Table S2, Supporting Information)^{29,30} and with similar calculations (B3LYP/6-311G(d,p)) performed on the constitutive molecule with the software Gaussian03.

The SPC model³¹ was used to describe the water molecule. This model describes the O and H atom of the rigid water molecule with a partial charge interacting through the Coulomb interaction. Moreover, the oxygen atom of the water molecule interacts through repulsion/dispersion interactions described using a Lennard-Jones potential. Cations and anions (LiCl, NaCl, and CsCl) of the electrolytes were treated as a sphere with a charge +1 and -1, respectively. In addition, each ion interacts through repulsion/dispersion interactions described using a Lennard-Jones potential. These Lennard-Jones parameters, which are presented in Table S2, Supporting Information, were taken from refs 32–34. Interactions between the atoms of water, atoms of the T-channel, and the ions include the Coulombic interaction and the dispersion interaction together with a repulsive interaction. The energy $U_k(r_k)$ of ion or atom k at position r_k is

$$U_k(r_k) = \sum_{j=\{OW,HW,X,Cl,O,N,C,H\}} \left\{ 4\epsilon_{jk} \left[\left(\frac{\sigma_{jk}}{r_{jk}} \right)^{12} - \left(\frac{\sigma_{jk}}{r_{jk}} \right)^6 \right] + \frac{q_j q_k}{4\pi\epsilon_0 r_{jk}} \right\} \quad (1)$$

where $X = \text{Li, Na, or Cs}$ and r_{kj} is the distance between the atom or ion j (OW, HW, X, Cl, O, C, N, or H) and the atom k of the electrolyte. All interaction contributions were determined within a cutoff corresponding to one-half of the smallest box length ~12 Å. The Coulombic interaction was computed using

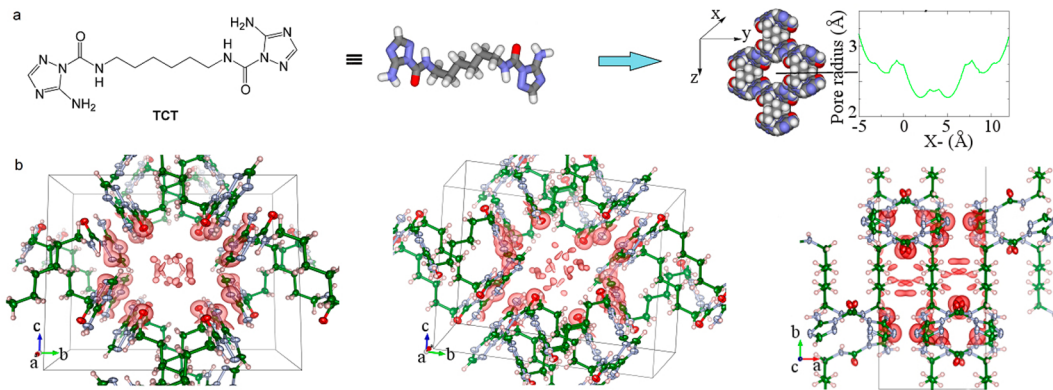


Figure 1. (a) Chemical formula and crystal structure of TCT compound self-assembling in T-channels with a pore void of small ($d = 2.5 \text{ \AA}$) and large ($d = 4 \text{ \AA}$) pore mouths. (b) Ellipsoid-and-stick representation of the crystal matrix of TCT with superimposed electron density isosurfaces (red) at the $1.3 \text{ e}/\text{\AA}^3$ level as calculated by the maximum entropy method³⁸ for the unit cell part $0 \leq x \leq 1$; $0.2 \leq y \leq 0.8$; $0.2 \leq z \leq 0.8$, and visualized by VESTA.³⁹ The maximum entropy method converged to reliability factors of $R_F = 0.0187$ and $wR_F = 0.0179$ using a fourth-order F-constraint. Most oxygen atoms in the channel are discrete entities, but this depends of course on the exact value of the isosurface level.

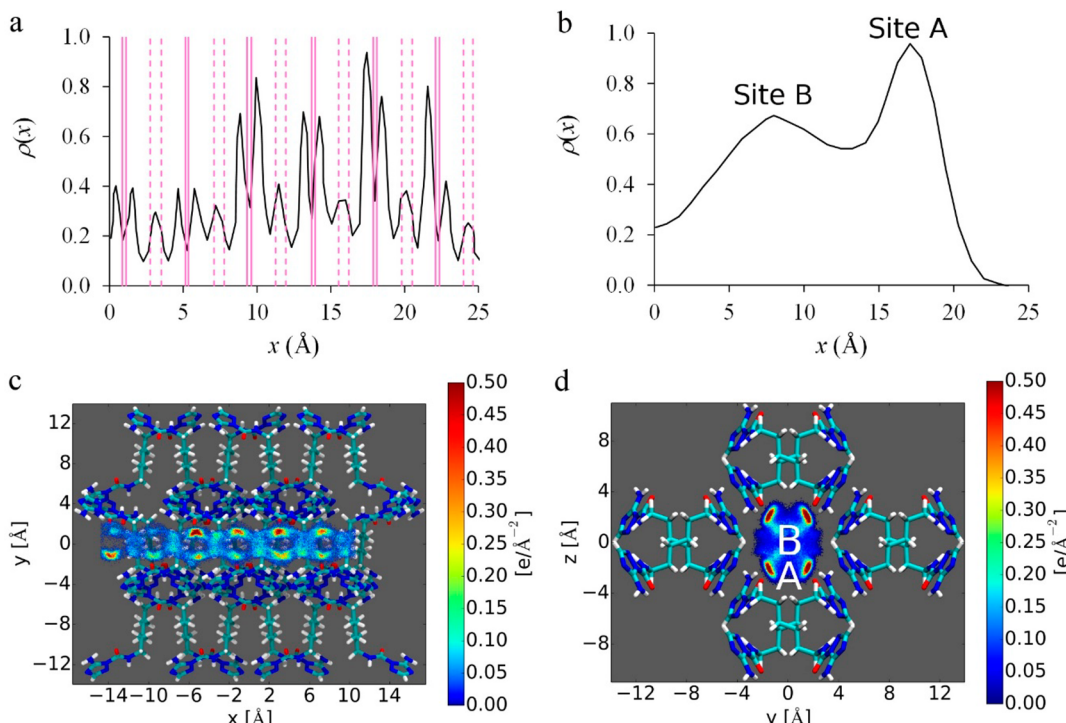


Figure 2. (Top) axial (left) and radial (right) density profiles of water confined in the T-channel as obtained by means of molecular simulation. The pink solid and dashed vertical lines correspond to the positions of the $-\text{C}=\text{O}$ and NH_2 groups, respectively, along the T-channel. The density ρ is in arbitrary units. For the axial density profile, ρ corresponds to the probability of finding a water molecule in a slice of volume unity at a position x along the pore axis. For the radial profile, ρ corresponds to the probability of finding a molecule in a volume unity between r and $r + dr$. (Bottom) absolute density in nm^{-3} given by the density profile multiplied by the number of water molecules per T-channel. Contour plots show the average density of water within the T-channel with the following color code: blue < green < yellow < orange < red.

the Ewald sum method with $\alpha = 0.22 \text{ \AA}^{-1}$, $k_A = 5$, $k_B = 7$, $k_C = 6$, where \vec{a} , \vec{b} , and \vec{c} , are the vectors of the simulation box. The interaction parameters for the substrate atoms are taken from AMBER force field for proteins.

The structure of water and electrolyte solutions in the T-channel was investigated using Monte Carlo simulations in the Canonical ensemble (MC).^{35,36} This technique is a stochastic method that simulates a system having a constant volume V (the T-channel with the adsorbed electrolyte solution), in equilibrium with a thermostat imposing its temperature T . Monte Carlo trial moves in the Canonical ensemble are

molecule translation or rotation and ion translation. These moves were attempted with an equal probability. Molecule translation and rotation and ion translation are accepted with a probability given in the frame of the Metropolis method:

$$P_{i,j} = \min\{1, \exp(-\beta\Delta U_{i,j})\} \quad (2)$$

where $\beta = 1/k_B T$ is the reciprocal temperature (k_B is the Boltzmann constant). $\Delta U_{i,j}$ is the change in the internal energy between the state i before the move and the state j after the move. The MC calculations were computed using a homemade program where the species are represented as rigid bodies. The

atomic positions of the substrate are maintained fixed during the MC simulations. Periodic boundary conditions were applied along the x , y , and z directions to avoid finite size effects. MC simulations were carried out for 5×10^7 trials for pure water and for 2×10^7 trials for electrolyte solutions. Configurations were stored each 10^4 trials. When the thermodynamic quantities were averaged, the first configurations were discarded as they correspond to an equilibration step.

3. RESULTS AND DISCUSSION

3.1. X-ray Structure of TCT. The unit cell is made of 12 molecules of TCT and 6 water molecules. Analysis of the crystals reveals homomeric H-bonding associations of the triazole moieties.³⁷ The intertwined TCT strands in the structure form double-helix by two $-\text{CONH}\cdots\text{N}_{\text{Im}}$ H-bonds ($d_{\text{N-H}} = 2.28 \text{ \AA}$) of the terminal T units, which present an unusual tetrahedral geometry (because double H-bond motifs are usually planar) (Figure 1). The successive tetrahedral H-bonding sequences strongly enforce the double-helical winding of the strand, which allows considerable overlap between the central hydrophobic chains of the monomers. The stiffness of the double helix formed by the TCT molecules arises from a combination of H-bonding and hydrophobic interactions and may be associated with the stable oligomers observed in solution over a large concentration domain.²²

The self-assembly of TCT molecules leads to hourglass T-channels with alternating small ($d = 2.5 \text{ \AA}$) and large ($d = 4 \text{ \AA}$) pore mouths (Figure 1). The inner pore presents an inversion plane with hypersurfaces of opposite chirality (half-superior and half-inferior). The water molecules confined within the T-channel are ordered with two preferential adsorption sites corresponding to $-\text{C=O}\cdots\text{H}_w$ and $-\text{NH}\cdots\text{O}_w$ H-bonds. They are arranged into approximately helical arrays, and their position is consistent with the diastereoisotopic pattern of the double helical T-channel. The electron density map of water within the crystal structure of TCT suggests that they should exhibit water disorder/motion (see Methods for a detailed discussion).

3.2. Molecular Structure of Water Confined within T-Channels. To shed light on the structure and ordering of water molecules within the T-channel, we performed Monte Carlo molecular simulations of water adsorbed within the experimentally determined structure. Two water molecules were adsorbed per T-channel. Considering that there are two channels per unit cell and that our simulation box has a length of 25.41 \AA (3 times the crystallographic parameter $a = 8.47 \text{ \AA}$), there are 12 water molecules in the simulation box (which is less than the experimental value). The simulated axial and radial density profiles in Figure 2 reveal significant positional ordering of water within the T-channel. Figure 2 also shows the simulated contour plots in the planes (x, y) and (y, z) of the density of water to illustrate the positions of water confined in the T-channel (these contour plots are integrated over the third direction). For the sake of clarity, we also show in the contour plots the skeleton of the T-channel, which is represented by silver, red, and blue sticks that correspond to the bonds between the C, O, and N atoms, respectively. The density at $r = 0$ is very low as there are nearly no water molecules in the center of the T-channel. The two marked density peaks observed at $r \sim 1.0$ and 2.1 \AA correspond to two layers of confined water. These two preferential positions are referred to as site A (in strong H-bonding interaction with the $-\text{C=O}$

groups) and site B (corresponding to water molecules interacting with the amino groups) (Figure 2).

This situation corresponding to a water molecule interacting with an oxygen atom of the carbonyl groups is clearly seen in the contour plot in the (y, z) plane shown in Figure 2 (position A). The second set of density peaks along the pore axis shows smaller peaks located between two successive sets of carbonyl groups. The subtle local ordering of water confined in the T-channel, which is characteristic of water confined in nanopores or in the vicinity of surfaces,^{40–44} suggests that its properties significantly differ from their bulk counterpart.

Figure 3 shows the pair correlation functions $g(r)$ ^{45,46} between the O_w and H_w of water and between the atoms of

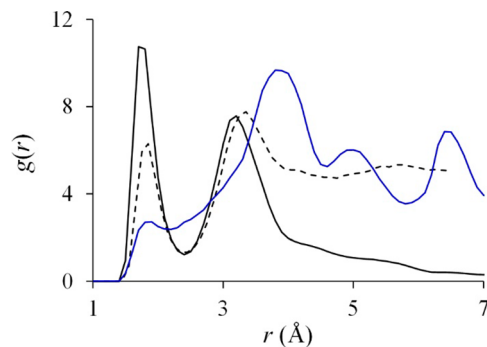


Figure 3. Pair correlation functions $g(r)$ between the H_w of water and the O of the T-channel surface (solid blue line), between the O_w and H_w of confined water (solid black line), and between the O_w and H_w of bulk water (dashed black line).

water and the oxygen atoms of the T-channel (O_S). The $g(r)$ between two atoms A and B is proportional to the probability of having A between r and $r + dr$ from B. The $g(r)$ function is related to the inverse Fourier transform of the structure factor $S(q)$ as determined from neutron or X-ray scattering.⁴⁷

The pair correlation functions between O_w and H_w exhibit short-range positional order, which is characteristic of a liquid phase. The first peak observed at a distance about $r \sim 1.8 \text{ \AA}$ corresponds to hydrogen bonding. As seen in Figure 3, such a distance is identical to what is obtained for bulk water. The first peak at a distance about $r \sim 1.8 \text{ \AA}$ in the $g(r)$ function between H_w and O_S atoms in water corresponds to the formation of hydrogen bonds between the water molecules and the oxygen atoms of the carbonyl groups of the T-channel. The amplitude of this peak $\sim 2.5–3$ is much smaller than that observed in confined water ~ 12.5 between O_w and H_w . The less significant hydrogen bonding for water with the oxygen atoms of the carbonyl groups is due to steric effects that prevent more than one water molecule from approaching the T-channel surface (steric interaction with other surface atoms). Moreover, these results suggest larger correlations between water molecules interacting with the neighboring water than for those interacting with carbonyl groups at the T-channel surface. The $g(r)$ function between O_S and H_w exhibits a second peak at a distance of 4 \AA , corresponding to the correlation between water molecules. The number $N_{2S} \sim 1$ of water molecules in interaction with the first closest carbonyl groups is readily obtained from the number of water in a sphere of radius $r = 4.5 \text{ \AA}$. Given that a T-channel contains 12 oxygen atoms and $N = 6$ adsorbed water molecules, the fact that $N_{2S} \sim N/6$ shows that each molecule is able to interact with two oxygen atoms.

We also investigated the dielectric structure and ordering of water within the T-channel. The density contour plots of water show two possible orientations: (a) in the upper part of the T-channel, the dipole of the water molecules is orientated along the positive axis and (b) in the lower part of the T-channel, the dipole of the water molecules is orientated along the negative axis (Figure 4). The dipolar orientation of the confined water

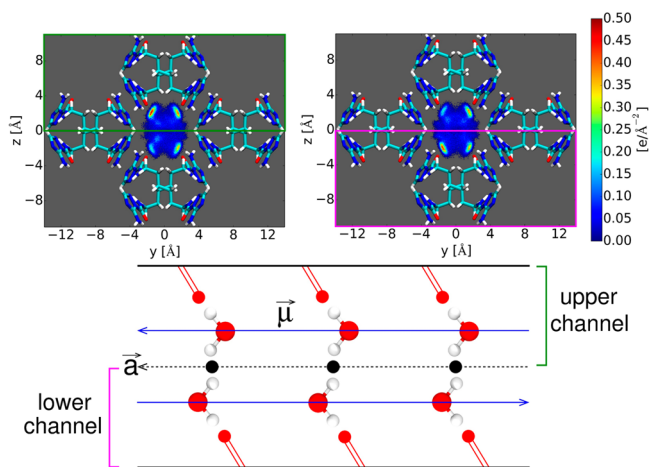


Figure 4. (a) Density contour plot of water (left) with $\mu_x < 0$ (i.e., dipole toward the direction $-\vec{a}$) and (right) with $\mu_x > 0$ (i.e., dipole pointing toward the direction \vec{a}). The density increases according to the following color code: blue < green < yellow < orange < red. The T-channel is shown for the sake of clarity. The orange and green boxes correspond to the regions referred to as the lower and upper parts of the T-channel in what follows and in the main text. (b) Schematic representation of the T-channel where one can distinguish the upper and lower parts mentioned above. The red spheres are the oxygen atoms of the $-\text{C}=\text{O}$ groups at the T-channel surface. The black spheres are the symmetry inversion centers, and the dashed vector indicates the pore axis (aligned with the axis \vec{a}). The blue vectors indicate the global dipolar orientation of water in the lower and upper regions.

molecules is mostly imposed by the $-\text{C}=\text{O}$ groups at the surface of the channel. Indeed, due to the inversion centers located between two successive sets of $-\text{C}=\text{O}$ groups, the oxygen atoms in the lower part of the pore toward the positive axis while the oxygen atoms in the upper part point toward the negative axis. Of course, this result was expected because confined water must respect the inversion center symmetry imposed by the host structure. Consequently, this finding should not be considered as a result in itself.

Figure S2 of the Supporting Information shows the components $\mu_x(x)$ of the average dipole moment $\vec{\mu}$ of water as a function of the position x along the T-channel axis (μ_x is the dipole component along the channel axis). μ_x oscillates with a period about 4.2 Å, which corresponds to the distance between two successive sets of oxygen atoms at the T-channel surface (carbonyl groups). Let x_{O}^- and x_{O}^+ be the lowest and highest x positions along the T-channel axis of two closest oxygen atoms (corresponding to one of the double solid vertical lines shown in Figure S2 of the Supporting Information). μ_x is negative and positive for $x \lesssim x_{\text{O}}^-$ and $x \gtrsim x_{\text{O}}^+$.

A similar but less pronounced behavior is observed around the positions x_{N}^- and x_{N}^+ of the nitrogen atoms of the amino groups; indeed, at equal distance between two sets of carbonyl groups, a second maximum in the absolute value of μ_x is

observed. This second preferential orientation ordering corresponds to water molecules interacting with the hydrogen atoms of the amino groups at the T-channel surface. These results show that the average dipole orientation of confined water is driven by both the oxygen atoms belonging to the carbonyl groups and the hydrogen atoms of the amino groups of the T-channel surface. We note that this surface-induced orientation ordering is consistent with the positional ordering observed in the density profiles (Figure 2). To further investigate the dipole and local orientation of the confined water molecules, we calculated the average angle φ defined as the angle of the average dipole $\vec{\mu}$ in the plane (y, z) (i.e., the plane perpendicular to the T-channel axis x):

$$\varphi = a \cos\left(\frac{\mu_y}{\mu \sin \theta}\right) \quad (1)$$

where μ_y is the component of $\langle \vec{\mu} \rangle$ along the axis y and θ is the azimuthal angle in cylindrical coordinates. Figure S2 in the Supporting Information also shows φ as a function of the position x along the T-channel axis. φ oscillates in a periodic fashion between -150° and $+150^\circ$. As in the case of μ_x , the period in the oscillations of φ is about 4.2 Å. Again, this value corresponds to the distance between two successive sets of oxygen and nitrogen atoms at the T-channel surface. This result shows that the average dipole orientation in the plane perpendicular to the T-channel axis is also driven by the interaction with the atoms of the functional groups of the surface. The results above emphasize that the average dipole orientation (given by the functions $\mu_x(x)$ and $\varphi(x)$) is imposed by the positions of the carbonyl and amino groups at the T-channel surface. This corresponds to a surface-induced polarization of confined water. Such an orientational ordering of confined water imposed by the pore surface is similar to what has been already observed in the case of water in carbon nanotubes.^{13,46,48–50} Given the symmetry of the T-channel atoms along the x axis, we expect confined water to have particular properties in terms of dipolar and local orientation. From the data shown until now, the following can be concluded:

- (1) There are two possible orientations for the confined water molecules inside meso-chiral T-channels: in the upper part of the channel, the net-dipole of the water molecules is oriented along the channel axis with a positive value, while in the lower part of the T-channel, the dipoles of the water molecules are oriented along the channel axis with a negative value.
- (2) This orientational ordering of water confined within the T-channel is imposed by the oxygen atoms at the surface of the host system. Indeed, due to the symmetry inversion centers located in the pore between two successive sets of carbonyl groups (black dots in Figure 4), the oxygen atoms in the lower part of the T-channel point toward the pore center and the positive direction of the pore axis while the oxygen atoms in the upper part of the T-channel point toward the pore center and the negative direction of the pore axis.

3.3. Molecular Structure of Confined Electrolytes in the T-Channel. To elucidate the behavior of confined electrolyte solutions, Monte Carlo molecular simulations were performed for ions (i.e., LiCl, NaCl, CsCl) located within the T-channel in the presence of $N = 6$ water molecules. Figure 5 shows contour plots in the (x, y) and (y, z) planes of the

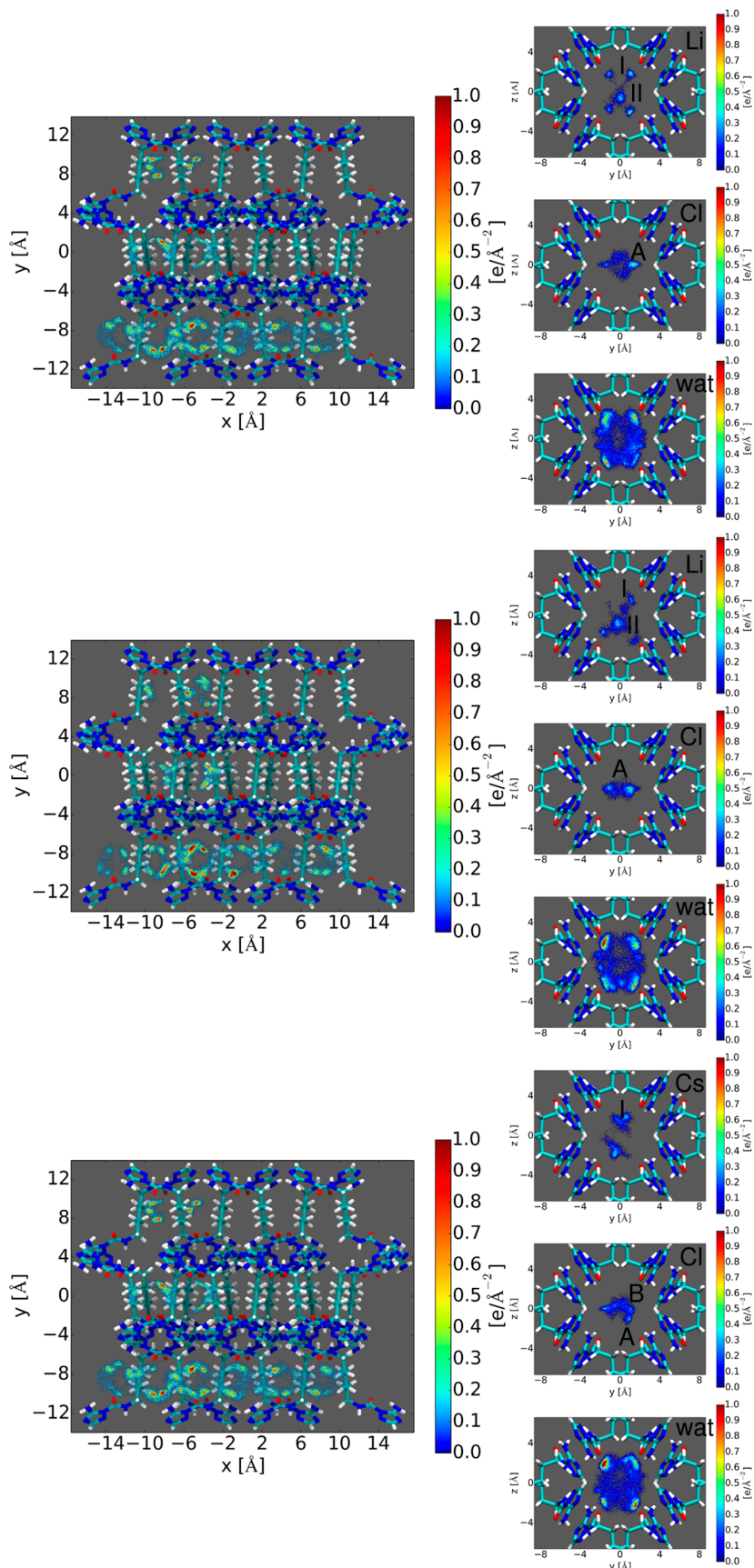


Figure 5. Density contour plots showing for (top) Li⁺, (middle) Na⁺, and (bottom) Cs⁺ cations. The left panel shows densities projected on the (x,y) plane. For each projection, three channels can be distinguished; they are used to show the cation (top channel), the anion (middle channel), and water (bottom channel) densities. The three channels are then depicted on the right panel when projected on the (y,z) plane. LiI and LiII, NaI and NaII, and CsI indicate the sites for Li⁺, Na⁺, and Cs⁺ cations in the T-channel (top). (Middle) Density contour plots showing the average density

Figure 5. continued

of Cl^- anions. CIA and ClB are the two sites for Cl^- in the T-channel. (Bottom) density contour plots for water in the T-channel. The density increases according to the following color code: blue < green < yellow < orange < red. The T-channel is shown for the sake of clarity.

density for Li^+ , Na^+ , Cs^+ , and Cl^- in the T-channel. The location of the cations significantly depends on their size through a subtle interplay between repulsive and attractive interactions with the T-channel surface. The radial density contour plot for Li^+ exhibits a layered structure with two layers located at $r = 0.15$ and 1.75 \AA (these values were estimated from radial density profiles that are not shown here for the sake of clarity and brevity). The first maximum corresponds to Li^+ located close to the surface, and the second maximum corresponds to Li^+ in the center of the T-channel (Li^I and Li^{II} , respectively, in Figure 5a). The radial density for Na^+ also shows two maxima located at 0.55 and 1.55 \AA , which are slightly shifted compared to those for Li^+ due to larger steric repulsion between the sodium cations (Na^I and Na^{II} , respectively, in Figure 5b). Finally, the radial density for Cs^+ exhibits a single peak located at 1.3 \AA . Given its large size, Cs^+ can only occupy one position between the center and the T-channel surface (Cs^I in Figure 5c). The radial density also shows that chloride anions form a layer close to the center of the channel. The position of this layer moves toward the T-channel center as the size of the cation increases, due to repulsion between the cations and T-channel atoms. In the case of CsCl , this layer corresponding to Cl^- anions subdivides into two layers. The first layer corresponds to a position in the vicinity of the surface, and the second layer corresponds to a position close to the T-channel center. Figure 6 shows the $g(r)$

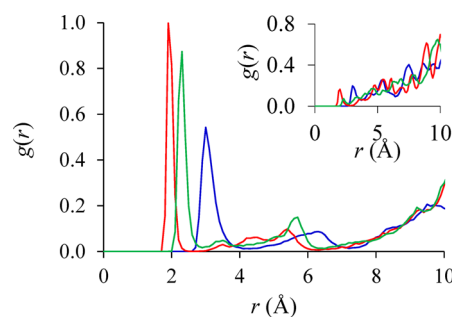


Figure 6. Pair correlation functions $g(r)$ between $X = \text{Li}^+$ (red lines), Na^+ (green lines), and Cs^+ (blue lines) and the oxygen atoms of water. The inset shows the same correlation functions between O_w and the O_s of the surface.

functions between Li^+ , Na^+ , and Cs^+ cations and O_w . The first peak in the $g(r)$ function between the cations and O_w is located at a distance 1.9 \AA for Li^+ , 2.3 \AA for Na^+ , and 3.0 \AA for Cs^+ . These values are slightly lower (by $0.1\text{--}0.2 \text{ \AA}$) than those obtained in experiments⁴⁸ and simulations^{45,51–56} for bulk alkali metal chloride solutions. The fact that the cations and oxygen atoms are closer can be explained by the larger salt concentration in our simulations ($\sim 9 \text{ mol/L}$) compared to those considered in the works cited above ($\sim 0.1\text{--}3 \text{ mol/L}$). This interpretation is supported by experimental and theoretical results obtained for highly concentrated aqueous solutions.^{57–60} The amplitude of this peak corresponding to the cation/oxygen positional correlation is large $\sim 0.5\text{--}1$ (depending on the cation type). As expected, the number of solvating water molecules around a cation (which corresponds to the

area of the first peak in the $g(r)$ function) increases with the cation size, in agreement with previous results reported in the literature.^{45,48,61–63} On the contrary, the amplitude of the peak decreases as the size of the cation increases as previously reported;⁶⁴ the positional ordering of water molecules cannot be maintained as the size of the solute increases.⁶⁵

Figure 6 shows the pair correlation functions $g(r)$ between the cations and oxygen atoms O_s of the carbonyl groups at the T-channel surface. The cation positions are correlated with the positions of the O atoms at the T-channel surface as a marked peak is observed in the pair correlation function between cations and O_s . These positions are similar to those observed in the $g(r)$ function between the cations and O_w . This observation is consistent with the fact that similar interactions are at play between these sets of atoms and cations. In contrast, the amplitudes for this peak between the cations and O_s is between 3 and 10 times lower than those for the corresponding peak between the cations and O_w . This result shows that the interactions between the cations and the water molecules are predominant, compared to the interactions between the cations and the surface oxygen atoms. This interpretation in terms of hydrophobic effect is supported by the water–water pair correlation functions (results not shown) showing that the positional ordering of the water molecules in the T-channel decreases with increasing the size of the cation.

Figure 7 shows the orientation φ of the average dipole moment $\vec{\mu}$ along the axis of the T-channel in the presence of the pairs of anions and cations M^+Cl^- (with $\text{M}^+ = \text{Li}^+$, Na^+ , and Cs^+). As in the case of pure water confined in the T-channel, φ oscillates in a periodic way between -150° and $+150^\circ$. The

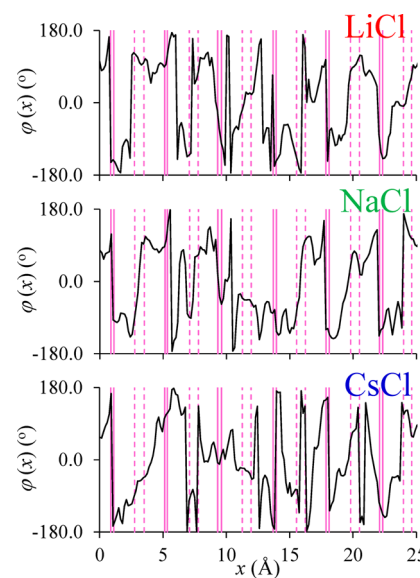


Figure 7. Angle φ between the average dipole $\vec{\mu}$ of water in the plane (y, z) , as a function of the position x along the T-channel axis, in the presence of the ion pairs: (top) LiCl , (middle) NaCl , and (bottom) CsCl . The pink solid and dashed vertical lines correspond to the positions of the surface oxygen atoms and the surface nitrogen atoms along the T-channel, respectively.

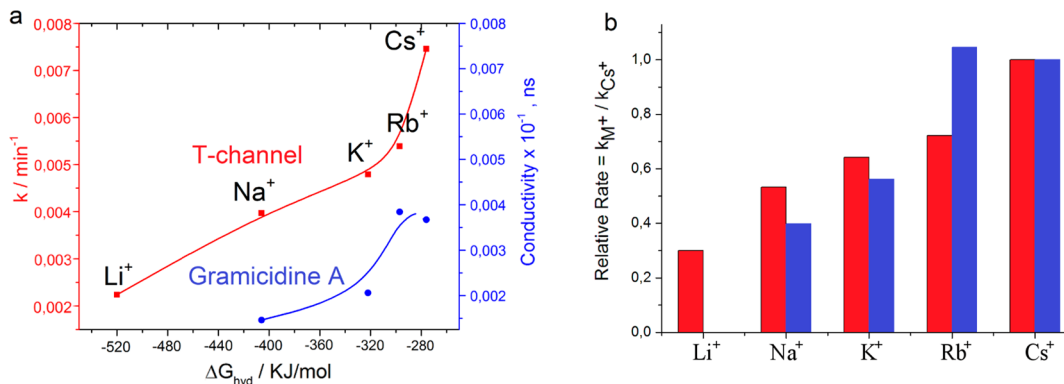


Figure 8. Bilayer membrane transport experiments. (a) Transport activities expressed as rate constants through T-channels (red) and as conductivity of Gramicidin A (blue), as a function of the dehydration energy of alkali metal cations, as reported in ref 67. These data show different increasing single-order exponential and saturation behaviors. (b) Relative transport rates of alkali metal cations using the Cs^+ activity as reference.

period in such an alternative orientation ordering of φ is about 4.2 Å, which corresponds to the distance between two successive sets of oxygen atoms and nitrogen atoms at the channel surface. This result shows that, even in the presence of ions, the average dipole orientation of water in the plane perpendicular to the T-channel axis is driven by the interaction with the atoms of the functional groups of the surface. In other words, despite the strong Coulombic water/ion interaction, water remains significantly ordered in the T-channel. Although the organization of confined water is observed for all cations, the distributions in Figure 7 become noisier upon increasing the cation size. This result shows that the orientation ordering of confined water is less marked as the cation becomes bigger. The molecular simulations above provide important insights into the structure of confined water and electrolyte solutions (alkali metal chlorides) in the T-channels. The T-channel accommodates two helical layers that occupy well-defined positions near carbonyl and amino groups of the T-channel. The confined system can be described as the sum of the two regions, which are separated by the plane (x, z) cutting in half the T-channel (we recall that x is the direction along the T-channel axis). One half of the channel porous space is occupied by aligned water molecules with their dipole upward with respect to \vec{a} . The other half of the channel porous space is filled with aligned water molecules with their dipole aligned with the direction $-\vec{a}$.

3.4. Bilayer Membrane Transport Experiments of Alkali Metal Cations. In this section, we present the bilayer membrane transport experiments of a series of alkali metal cations through T-channels. Previous transport experiments have shown that the T-channel presents very interesting ionic conduction. For alkali metal ions, transport activity of the T-channel increases according to the Eisenman sequence I:⁶⁶ $\text{Li}^+ < \text{Na}^+ < \text{K}^+ < \text{Rb}^+ \ll \text{Cs}^+$ (Figure 8). Such an order, which is identical to that observed for Gramicidin A, indicates that transport is driven by the energy penalty corresponding to ion dehydration.

In the case of Gramicidin A, cation/water transport through the narrow channel is known to occur via single-file diffusion. In such a process, the net dipole moment of oriented water molecules is of utmost importance because it influences the ionic pumping effect, depending on the ion position within Gramicidin A. However, a substantial contribution to cation selectivity, which follows the order $\text{Na}^+ < \text{K}^+ < \text{Rb}^+ \sim \text{Cs}^+$,⁶⁷ arises through ion exchange between hydrated ions in water

and dehydrated (confined) ions interacting with hydrophilic moieties pointing toward the transported cation and located on the inner pore walls (Figure 8). This implies that dehydration must occur so that the alkali metal cations enter the pores. For Gramicidin A, the free energy cost upon dehydration is thermodynamically compensated by the complexation free energy gained when the cation is located in the pore, allowing the ions to penetrate the channel. The fact that transport activities for Rb^+ and Cs^+ are very similar suggests that the balance between hydration and complexation energies is optimal for these ions.

Ion transport in the T-channel also follows the order $\text{Li}^+ < \text{Na}^+ < \text{K}^+ < \text{Rb}^+$ (Figure 8), which indicates that transport is also driven by the interplay between complexation and hydration energies. However, in contrast to the results for Gramicidin A, the T-channel displays enhanced transport for Cs^+ with respect to the other cations including Rb^+ . Moreover, the transport activities for the T-channel are much larger than those for Gramicidin A. Altogether, these results suggest that transport is strongly affected by the significant structural ordering of water confined in the T-channel. In particular, it can be assumed that optimal transport properties are shifted toward larger ions compared to the case of Gramicidin A because of the net dipole of water confined in the T-channel. For instance, once dehydrated from their bulk state, cations can permeate within the T-channel through subsequent hydration/dehydration along the oriented water wires. The orientation of the water wires can also account for the ion translocation activation because the oriented water clusters act as dielectric lubricants at the T-channel surface. To clarify this issue, further work is needed with rigorous assessment of hydration, complexation, and dielectric energies.

4. CONCLUSION

Dynamically organized water clusters have been considered as an amazing source of inspiration for understanding complex biological scenarios. Structured water and derived physical theories have been the sources of continuous controversies. However, it should be stressed that moving from conventional bulk water to confined water nanovessels is not simply just a matter of size, as the behavior of water confined in inner nanospaces is quite different from their behavior as unique molecular water, as well as under bulk conditions. “Compartmentalization” is also an important process in biology because many physiological processes occur under confined conditions

such as ionic/water transport through narrow pores, enzymatic reactions, etc.

The strong orientational ordering of water at the surface of phospholipid bilayers⁶⁸ or biomolecular systems⁶⁸ renders its properties different from those of bulk water. Water–water interactions together with specific interactions with the biosurfaces will determine its dipolar orientation and most probably specific dielectric properties influencing biological recognition at biointerfaces.¹⁰ Moreover, oriented water dipoles strongly determine the selectivity across the biological pores like Gramicidin A¹⁰ and Aquaporins.⁴

We suggest here that confined oriented water plays a biolubricant role in the selectivity of ionic transport across simpler artificial pores.^{4,6,7} The water molecules within the T-channel are partially disordered and occupy two positions. Their positioning is consistent with the diastereoisotopic pattern of the double helical T-channel observed in X-ray structures. Further theoretical Monte Carlo simulations shed light on important behaviors of the dynamic structure of water and electrolyte solutions (alkali metal chlorides) confined in T-channels. The strong interaction between water and the surface T-channel groups imposes surface-induced polarization of confined water, having dielectric properties that differ significantly from their bulk counterparts. Despite the strong confinement of water in the T-channel and its interaction with the surface, significant ion hydration remains possible under confined conditions (as illustrated by the strong correlation peaks in the water/ion pair correlation functions). However, even in the presence of ions, confined water remains significantly self-organized in the T-channel and still exhibits alternative orientation ordering. When analyzed together, these two findings suggest that, despite significant orientational ordering of confined water, the ions remain hydrated in the sense that they are still surrounded by an important number of water molecules. On the contrary, such hydration is necessarily specific to this confined system because the structure of confined water in the T-channel departs from that of bulk water.

Our findings show that natural systems can be biomimicked using artificial materials with similar functions. The T-channel system reported in this paper provides remarkable combinations of functions very close to those encountered in natural systems, and the dynamic orientational behaviors of confined water can be elucidated using such simplified systems. On the basis of the similarities between transport in Gramicidin A and the T-channel, we conclude that the balance between hydration and complexation energies of the confined cations is the dominant contribution to selectivity/transport observed within the T-channel. However, the increased transport activities for the T-channel (together with the fact that large ions are also translocated more efficiently) suggest that the helical water wires act as lubricant, which influences ion conduction. Such correlations between two asymmetric properties (the *chiral pore surface* and *oriented dipolar water wires*) allow envisioning novel translocation mechanisms that parallel to natural ion-pumping processes. Conversely, the dynamical yet slow molecular-scale hydrodynamics of confined water is of crucial relevance for understanding complex functions at the heart of interesting biological scenarios.

ASSOCIATED CONTENT

S Supporting Information

Experimental and molecular simulation parameters, including preparation quantities, atomic models, atomic partial charges, and graphs of μ_x and ϕ vs position x . The Supporting Information is available free of charge on the ACS Publications website at DOI: 10.1021/acs.jpcb.5b03322.

AUTHOR INFORMATION

Corresponding Authors

*M. Barboiu. E-mail: mihail-dumitru.barboiu@univ-montp2.fr.
*B. Coasne. E-mail: coasne@mit.edu.

Notes

The authors declare no competing financial interest.

ACKNOWLEDGMENTS

This work was conducted within the framework of DYNANO, PITN-GA-2011-289033 (www.dynano.eu) and LabEx Chémisyst, Pole Chimie Balard of Montpellier.

REFERENCES

- (1) Cukierman, S. Proton Mobilities in Water and in Different Stereoisomers of Covalently Linked Gramicidin A Channels. *Biophys. J.* **2000**, *78*, 1825–1834.
- (2) Roux, B. Computational Studies of the Gramicidin Channel. *Acc. Chem. Res.* **2002**, *35*, 366–375.
- (3) Allen, T. W.; Andersen, O. S.; Roux, B. Energetics of Ion Conduction through the Gramicidin Channel. *Proc. Natl. Acad. Sci. U. S. A.* **2004**, *101*, 117–122.
- (4) Agre, P. Aquaporin Water Channels (Nobel Lecture). *Angew. Chem., Int. Ed.* **2004**, *43*, 4278–4290.
- (5) Gravelle, S.; Joly, L.; Detcheverry, F.; Ybert, C.; Cottin-Bizonne, C.; Bocquet, L. Optimizing Water Permeability through the Hourglass Shape of Aquaporins. *Proc. Natl. Acad. Sci. U. S. A.* **2013**, *110*, 16367–16372.
- (6) MacKinnon, R. Potassium Channels and the Atomic Basis of Selective Ion Conduction (Nobel Lecture). *Angew. Chem., Int. Ed.* **2004**, *43*, 4265–4277.
- (7) Pinto, L. H.; Dieckmann, G. R.; Gandhi, C. S.; Papworth, C. G.; Braman, J.; Shaughnessy, M. A.; Lear, J. D.; Lamb, R. A.; DeGrado, W. F. A Functionally Defined Model for the M-2 Proton Channel of Influenza A Virus Suggests a Mechanism for its Ion Selectivity. *Proc. Natl. Acad. Sci. U. S. A.* **1997**, *94*, 11301–11306.
- (8) Hu, F.; Luo, W.; Hong, M. Mechanisms of Proton Conduction and Gating in Influenza M2 Proton Channels from Solid-State NMR. *Science* **2010**, *330*, 505–508.
- (9) Sharma, M.; Yi, M.; Dong, H.; Qin, H.; Peterson, E.; Busath, D. D.; Zhou, H.-X.; Cross, T. A. Insight into the Mechanism of the Influenza A Proton Channel from a Structure in a Lipid Bilayer. *Science* **2010**, *330*, 509–512.
- (10) Ball, P. Water as an Active Constituent in Cell Biology. *Chem. Rev.* **2008**, *108*, 74–108.
- (11) Zhong, D.; Pal, S. K.; Zewail, A. H. Biological Water: a Critique. *Chem. Phys. Lett.* **2011**, *503*, 1–11.
- (12) Pal, S. K.; Zewail, A. H. Dynamics of Water in Biological Recognition. *Chem. Rev.* **2004**, *104*, 2099–2123.
- (13) Koga, K.; Gao, G. T.; Tanaka, H.; Zeng, X. C. Formation of Ordered Ice Nanotubes inside Carbon Nanotubes. *Nature* **2001**, *412*, 802–805.
- (14) Muller, A. A.; Bogge, H.; Diemann, E. Structure of a Cavity-Encapsulated Nanodrop of Water. *Inorg. Chem. Commun.* **2003**, *6*, 52–53.
- (15) Yoshizawa, M.; Kusukawa, T.; Kawano, M.; Ohhara, T.; Tanaka, I.; Kurihara, K.; Niimura, N.; Fujita, M. Endohedral Clusterization of Ten Water Molecules into a "Molecular Ice" within the Hydrophobic

- Pocket of a Self-Assembled Cage. *J. Am. Chem. Soc.* **2005**, *127*, 2798–2799.
- (16) Gorbitz, C. H. Microporous Organic Materials from Hydrophobic Dipeptides. *Chem. - Eur. J.* **2007**, *13*, 1022–1031.
- (17) Alabarse, F. G.; Haines, J.; Cambon, O.; Levelut, C.; Bourgogne, D.; Haidoux, A.; Granier, D.; Coasne, B. Freezing of Water Confined at the Nanoscale. *Phys. Rev. Lett.* **2012**, *109*, 035701.
- (18) Alabarse, F. G.; Rouquette, J.; Coasne, B.; Haidoux, A.; Paulmann, C.; Cambon, O.; Haines, J. Mechanism of H_2O Insertion and Chemical Bond Formation in $\text{AlPO}_4 \cdot 54 \text{ xH}_2\text{O}$ at High Pressure. *J. Am. Chem. Soc.* **2015**, *137*, 584–587.
- (19) Le Duc, Y.; Michau, M.; Gilles, A.; Gence, V.; Legrand, Y.-M.; van der Lee, A.; Tingry, S.; Barboiu, M. Imidazole-Quartet Water and Proton Dipolar Channels. *Angew. Chem., Int. Ed.* **2011**, *50*, 11366–11372.
- (20) Barboiu, M. Artificial Water Channels. *Angew. Chem., Int. Ed.* **2012**, *51*, 11674–11676.
- (21) Barboiu, M.; Gilles, A. From Natural to Bio-Assisted and Biomimetic Artificial Water Channel Systems. *Acc. Chem. Res.* **2013**, *46*, 2814–2823.
- (22) Barboiu, M.; Le Duc, Y.; Gilles, A.; Cazade, P.-A.; Michau, M.; Legrand, Y.-M.; van der Lee, A.; Coasne, B.; Parvizi, P.; Post, J.; Fyles, T. An Artificial Primitive Mimic of the Gramicidin A Channel. *Nat. Commun.* **2014**, *5*, 4142.
- (23) Palatinus, L.; Chapuis, G. SUPERFLIP - a Computer Program for the Solution of Crystal Structures by Charge Flipping in Arbitrary Dimensions. *J. Appl. Crystallogr.* **2007**, *40*, 786–790.
- (24) Betteridge, P. W.; Carruthers, J. R.; Cooper, R. I.; Prout, K.; Watkin, D. J. CRYSTALS Version 12: Software for Guided Crystal Structure Analysis. *J. Appl. Crystallogr.* **2003**, *36*, 1487–1487.
- (25) van der Sluis, P.; Spek, A. L. BYPASS: an Effective Method for the Refinement of Crystal Structures Containing Disordered Solvent Regions. *Acta Crystallogr., Sect. A: Found. Crystallogr.* **1990**, *46*, 194–201.
- (26) Spek, A. L. Single-Crystal Structure Validation with the Program PLATON. *J. Appl. Crystallogr.* **2003**, *36*, 7–13.
- (27) Sidorov, V.; Kotch, F. W.; Abdurakhmanova, G.; Mizani, R.; Fettinger, J. C.; Davis, J. T. Ion Channel Formation from a Calix-4-Arene Amide that Binds HCl. *J. Am. Chem. Soc.* **2002**, *124*, 2267–2278.
- (28) Dovesi, R.; Saunders, V. R.; Roetti, C.; Orlando, R.; Zicovich-Wilson, C. M.; Pascale, F.; Civalleri, B.; Doll, K.; Harrison, N. M.; Bush, I. J. et al. *CRYSTAL06 User's Manual*; University of Torino: Torino, Italy, 2006.
- (29) Case, D. A.; Darden, T. A.; Cheatham, T. E.; Simmerling, C. L.; Wang, J.; Duke, R. E.; Luo, R.; Mertz, K. M.; Pearlman, D. A.; Crowley, M. et al. *AMBER 9*; University of California: San Francisco, USA, 2006.
- (30) Weiner, S. J.; Kollman, P. A.; Nguyen, D. T.; Case, D. A. An All Atom Force Field for Simulations of Proteins and Nucleic Acids. *J. Comput. Chem.* **1986**, *7*, 230–252.
- (31) Jorgensen, W. L.; Chandrasekhar, J.; Madura, J. D.; Impey, R. W.; Klein, M. L. Comparison of Simple Potential Functions for Simulating Liquid Water. *J. Chem. Phys.* **1983**, *79*, 926–935.
- (32) Dang, L. X. Development of Nonadditive Intermolecular Potentials using Molecular Dynamics: Solvation of Li^+ and F^- Ions in Polarizable Water. *J. Chem. Phys.* **1992**, *96*, 6970–6977.
- (33) Smith, D. E.; Dang, L. X. Computer Simulations of Cesium–Water Clusters: Do Ion–Water Clusters Form Gas-Phase Clathrates? *J. Chem. Phys.* **1994**, *101*, 7873–7881.
- (34) Dang, L. X. Computational Study of Ion Binding to the Liquid Interface of Water. *J. Phys. Chem. B* **2002**, *106*, 10388–10394.
- (35) Allen, M. P.; Tildesley, D. J. *Computer Simulation of Liquids*; Clarendon Press: Oxford, U.K., 1987.
- (36) Frenkel, D.; Smit, B. *Understanding Molecular Simulation*, 2nd ed.; Academic Press: New York, 2002.
- (37) Legrand, Y. M.; Michau, M.; van der Lee, A.; Barboiu, M. Homomeric and Heteromeric Self-Assembly of Hybrid Ureido-Imidazole Compounds. *CrystEngComm* **2008**, *10*, 490–492.
- (38) van Smaalen, S.; Palatinus, L.; Schneider, M. The Maximum-Entropy Method in Superspace. *Acta Crystallogr., Sect. A: Found. Crystallogr.* **2003**, *59*, 459–469.
- (39) Momma, K.; Izumi, F. VESTA 3 for Three-Dimensional Visualization of Crystal, Volumetric and Morphology Data. *J. Appl. Crystallogr.* **2011**, *44*, 1272–1276.
- (40) Alexiadis, A.; Kassinos, S. Molecular Simulation of Water in Carbon Nanotubes. *Chem. Rev.* **2008**, *108*, 5014–5034.
- (41) Hummer, G.; Rasaiah, J. C.; Noworyta, J. P. Water Conduction through the Hydrophobic Channel of a Carbon Nanotube. *Nature* **2001**, *414*, 188–190.
- (42) Noon, W. H.; Ausman, K. D.; Smalley, R. E.; Ma, J. P. Helical Ice-Sheets inside Carbon Nanotubes in the Physiological Condition. *Chem. Phys. Lett.* **2002**, *355*, 445–448.
- (43) Kolesnikov, A. I.; Zanotti, J. M.; Loong, C. K.; Thiyagarajan, P.; Moravsky, A. P.; Loutfy, R. O.; Burnham, C. J. Anomalously Soft Dynamics of Water in a Nanotube: A Revelation of Nanoscale Confinement. *Phys. Rev. Lett.* **2004**, *93*, 035503.
- (44) Mukherjee, B.; Maiti, P. K.; Dasgupta, C.; Sood, A. K. Strongly Anisotropic Orientational Relaxation of Water Molecules in Narrow Carbon Nanotubes and Nanorings. *ACS Nano* **2008**, *2*, 1189–1196.
- (45) Ansell, S.; Barnes, A. C.; Mason, P. E.; Neilson, G. W.; Ramos, S. X-ray and Neutron Scattering Studies of the Hydration Structure of Alkali Ions in Concentrated Aqueous Solutions. *Biophys. Chem.* **2006**, *124*, 171–179.
- (46) Egorov, A. V.; Komolkin, A. V.; Chizhik, V. I.; Yushmanov, P. V.; Lyubartsev, A. P.; Laaksonen, A. Temperature and Concentration Effects on Li^+ -Ion Hydration. A Molecular Dynamics Simulation Study. *J. Phys. Chem. B* **2003**, *107*, 3234–3242.
- (47) Head-Gordon, T.; Hura, G. Water Structure from Scattering Experiments and Simulation. *Chem. Rev.* **2002**, *102*, 2651–2669.
- (48) Soper, A. K.; Neilson, G. W.; Enderby, J. E.; Howe, R. A. Neutron-Diffraction Study of Hydration Effects in Aqueous Solutions. *J. Phys. C: Solid State Phys.* **1977**, *10*, 1793–1801.
- (49) Ramos, S.; Neilson, G. W.; Barnes, A. C.; Buchanan, P. An Anomalous X-Ray Diffraction Study of the Hydration Structures of Cs^+ and I^- in Concentrated Solutions. *J. Chem. Phys.* **2005**, *123*, 214501–214510.
- (50) Mason, P. E.; Ansell, S.; Neilson, G. W. Neutron Diffraction Studies of Electrolytes in Null Water: a Direct Determination of the First Hydration Zone of Ions. *J. Phys.: Condens. Matter* **2006**, *18*, 8437–8447.
- (51) Loeffler, H. H.; Mohammed, A. M.; Inada, Y.; Funahashi, S. Lithium(I) Ion Hydration: a QM/MM-MD Study. *Chem. Phys. Lett.* **2003**, *379*, 452–457.
- (52) Varma, S.; Rempe, S. B. Coordination Numbers of Alkali Metal Ions in Aqueous Solutions. *Biophys. Chem.* **2006**, *124*, 192–199.
- (53) Webb, M. B.; Garofalini, S. H.; Scherer, G. W. Use of a Dissociative Potential to Simulate Hydration of Na^+ and Cl^- ions. *J. Phys. Chem. B* **2009**, *113*, 9886–9893.
- (54) Mile, V.; Pusztai, L.; Dominguez, H.; Pizio, O. Understanding the Structure of Aqueous Cesium Chloride Solutions by Combining Diffraction Experiments, Molecular Dynamics Simulations, and Reverse Monte Carlo Modeling. *J. Phys. Chem. B* **2009**, *113*, 10760–10769.
- (55) Cazade, P. A.; Dweik, J.; Coasne, B.; Henn, F.; Palmeri, J. Molecular Simulation of Ion-Specific Effects in Confined Electrolyte Solutions Using Polarizable Forcefields. *J. Phys. Chem. C* **2010**, *114*, 12245–12257.
- (56) Cazade, P. A.; Hartkamp, R.; Coasne, B. Structure and Dynamics of an Electrolyte Confined in Charged Nanopores. *J. Phys. Chem. C* **2014**, *118*, 5061–5072.
- (57) Ansell, S.; DupuyPhilon, J.; Jal, J. F.; Neilson, G. W. Ionic Structure in the Aqueous Electrolyte Glass $\text{LiCl}_4 \text{ D}_2\text{O}$. *J. Phys.: Condens. Matter* **1997**, *9*, 8835–8847.
- (58) Degreve, L.; da Silva, F. L. B. Structure of Concentrated Aqueous NaCl Solution: a Monte Carlo study. *J. Chem. Phys.* **1999**, *110*, 3070–3078.

- (59) Bouazizi, S.; Nasr, S. Local Order in Aqueous Lithium Chloride Solutions as Studied by X-Ray Scattering and Molecular Dynamics Simulations. *J. Mol. Struct.* **2007**, *837*, 206–213.
- (60) Bouazizi, S.; Hammami, F.; Nasr, S.; Bellissent-Funel, M. C. Neutron Scattering Experiments on Aqueous Sodium Chloride Solutions and Heavy Water. Comparison to Molecular Dynamics and X-Ray Results. *J. Mol. Struct.* **2008**, *892*, 47–52.
- (61) Ohtomo, N.; Arakawa, K. Neutron-Diffraction Study of Aqueous Ionic-Solutions. 2. Aqueous-Solutions of NaCl and KCl. *Bull. Chem. Soc. Jpn.* **1980**, *53*, 1789–1794.
- (62) Ohtaki, H.; Radnai, T. Structure and Dynamics of Hydrated Ions. *Chem. Rev.* **1993**, *93*, 1157–1204.
- (63) Lee, S. H.; Rasaiyah, J. C. Molecular Dynamics Simulation of Ion Mobility. 2. Alkali Metal and Halide Ions using the SPC/E Model for Water at 25 Degrees. *C. J. Phys. Chem.* **1996**, *100*, 1420–1425.
- (64) Chandler, D. Interfaces and the Driving Force of Hydrophobic Assembly. *Nature* **2005**, *437*, 640–647.
- (65) Mancinelli, R.; Botti, A.; Bruni, F.; Ricci, M. A.; Soper, A. K. Perturbation of Water Structure due to Monovalent Ions in Solution. *Phys. Chem. Chem. Phys.* **2007**, *9*, 2959–2967.
- (66) Eisenman, G.; Horn, R. Ionic Selectivity Revisited - The Role of Kinetic and Equilibrium Processes in Non Permeation through Channels. *J. Membr. Biol.* **1983**, *76*, 197–225.
- (67) Pfeifer, J. R.; Reiss, P.; Koert, U. Crown Ether-Gramicidin Hybrid Ion Channels: Dehydration-Assisted Ion Selectivity. *Angew. Chem., Int. Ed.* **2006**, *45*, 501–504.
- (68) Cheng, J. X.; Pautot, S.; Weitz, D. A.; Xie, X. S. Ordering of Water Molecules between Phospholipid Bilayers Visualized by Coherent Anti-Stokes Raman Scattering Microscopy. *Proc. Natl. Acad. Sci. U. S. A.* **2003**, *100*, 9826–9830.